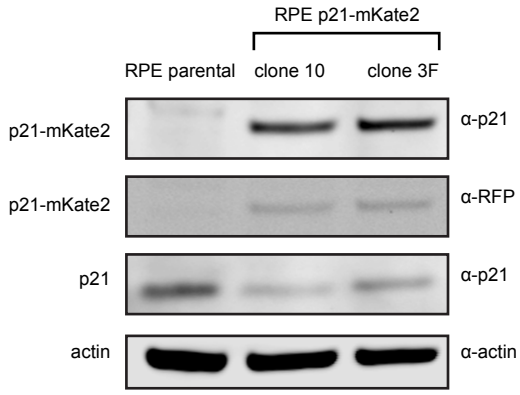

Figure S1. Endogenous fluorescent tagging of p21. *(Related to Main Text Fig. 3)*

Cells received 10Gy γ-irradiation. Protein samples were collected 24h post-DNA damage. Western blot confirms heterozygous endogenous tagging of p21 protein with the fluorescent protein mKate2 in two independently derived clones. Clone 10 is used in conjunction with CDK2 activity reporter DHB-mVenus in main text Fig. 4. Clone 3F is used to simultaneously quantify p53 and p21 dynamics in main text Figs. 3, 5.

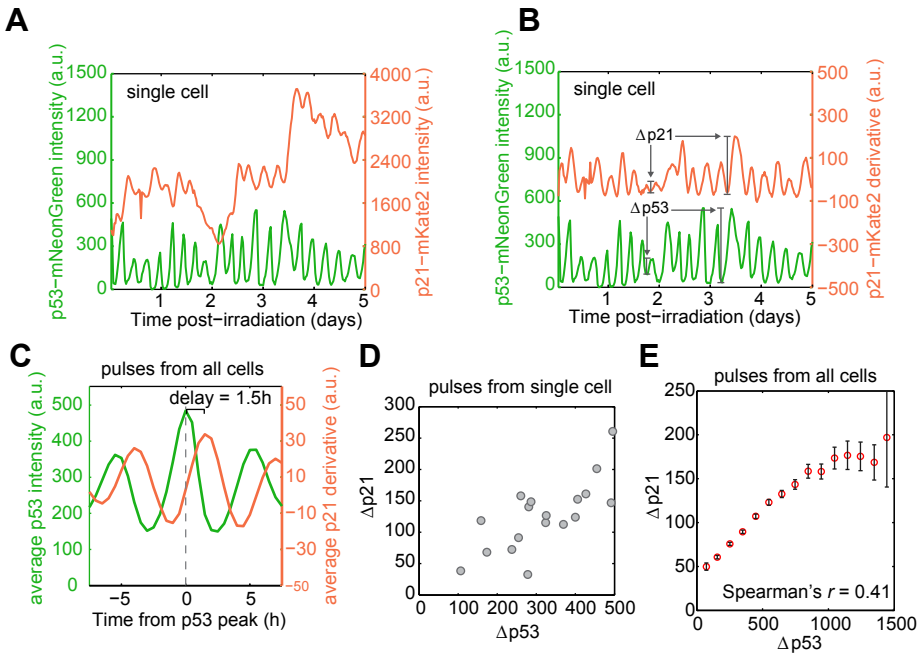

Figure S2. p21 protein dynamics inherit p53 dynamics. *(Related to Main Text Fig. 3)*

(A) Representative trajectory of a single cell exposed to 10Gy γ-irradiation (also shown in main text Fig. 2D).

(B) Trajectories of p53 and p21 derivatives calculated from traces shown in (A). Changes in p21 protein closely follow changes in p53 with a time delay.

(C) p53 and p21 derivative trajectories were aligned on the peak of individual p53 pulses. p21 derivative follows pulsatile p53 dynamics with a time delay of 1.5h.

(D) Correlation between p53 and p21 derivative pulse amplitude in a representative cell (shown in B).

(E) Average +/- s.e.m. p21 derivative amplitude as a function of p53 pulse amplitude.

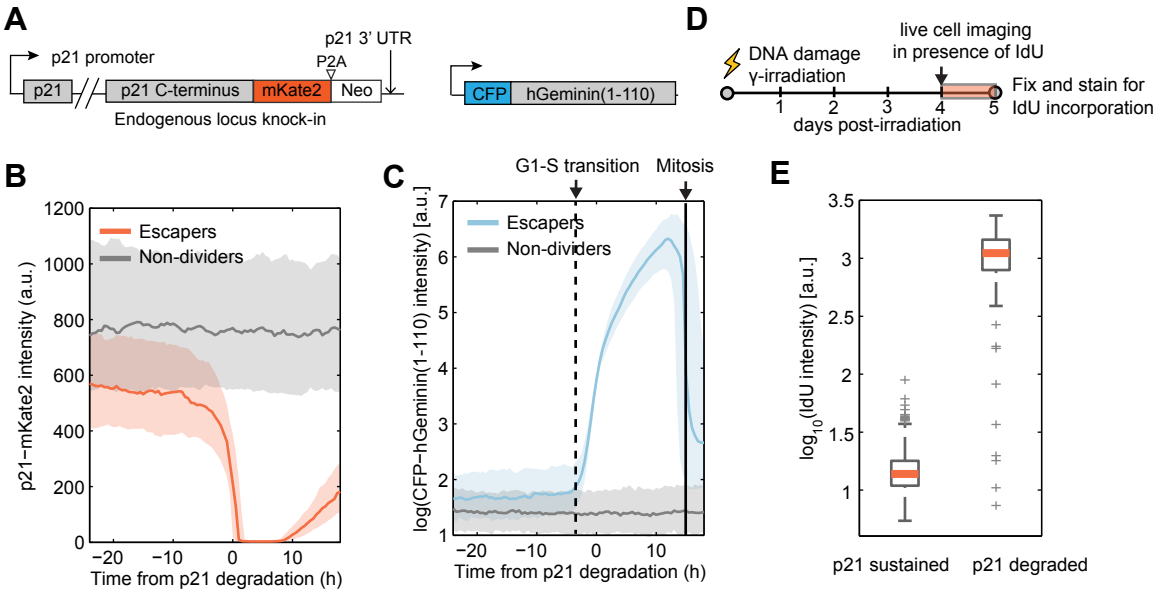

Figure S3. p21 is sharply degraded at the onset of G1-S transitions. *(Related to Main Text Fig. 4)*

(A) p21-mKate2 and CFP-hGeminin(1-110) allow quantification of p21 protein dynamics and cell cycle progression in individual cells after DNA damage.

(B) Individual escaper cells were aligned at the time p21 reaches baseline levels. Non-divider cells were randomly sampled to match timing of individual escape events. Bold lines and shaded areas represent median and interquartile range of p21-mKate2 trajectories.

(C) Quantification of CFP-hGeminin(1-110) reporter in relation to p21 degradation events. Escapers start accumulating CFP-hGeminin(1-110) concurrently with p21 degradation.

(D) Experimental timeline to determine the relationship between p21 degradation events and DNA replication. Cells were exposed to 4Gy γ-irradiation and imaged 4 days later in the presence of the thymidine analog IdU, for 24h. Cells were fixed and stained for IdU incorporation immediately after live cell imaging finished.

(E) Quantification of IdU signal intensity conditioned on whether a cell completely degraded p21 or maintained sustained levels in the course of live cell imaging experiment. Cells that degraded p21 incorporated IdU, corroborating that such degradation events correspond to G1-S transitions.

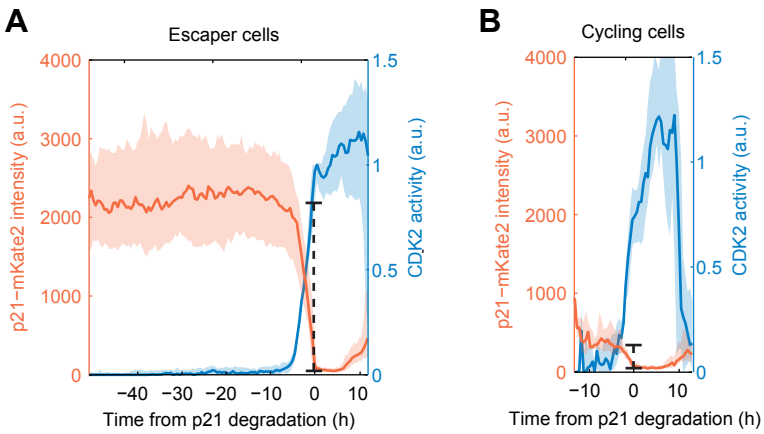

Figure S4. Escapers degrade p21 from a higher level than that observed during normal cycling. *(Related to Main Text Fig. 4)*

(A, B) p21 and CDK2 activity trajectories were aligned with respect to G1-S transitions in escapers (A) or cycling cells (B). Consistent with previous reports (Barr et al., 2017; Coleman et al., 2015), p21 is sharply degraded upon S-phase entry. However, the onset of p21 degradation is from a higher level in escapers than as compared to cycling cells. This suggests that while p21 accumulation after DNA damage is sufficient to establish cell cycle arrest, it is not sufficient to maintain such state for prolonged timescales in escapers.

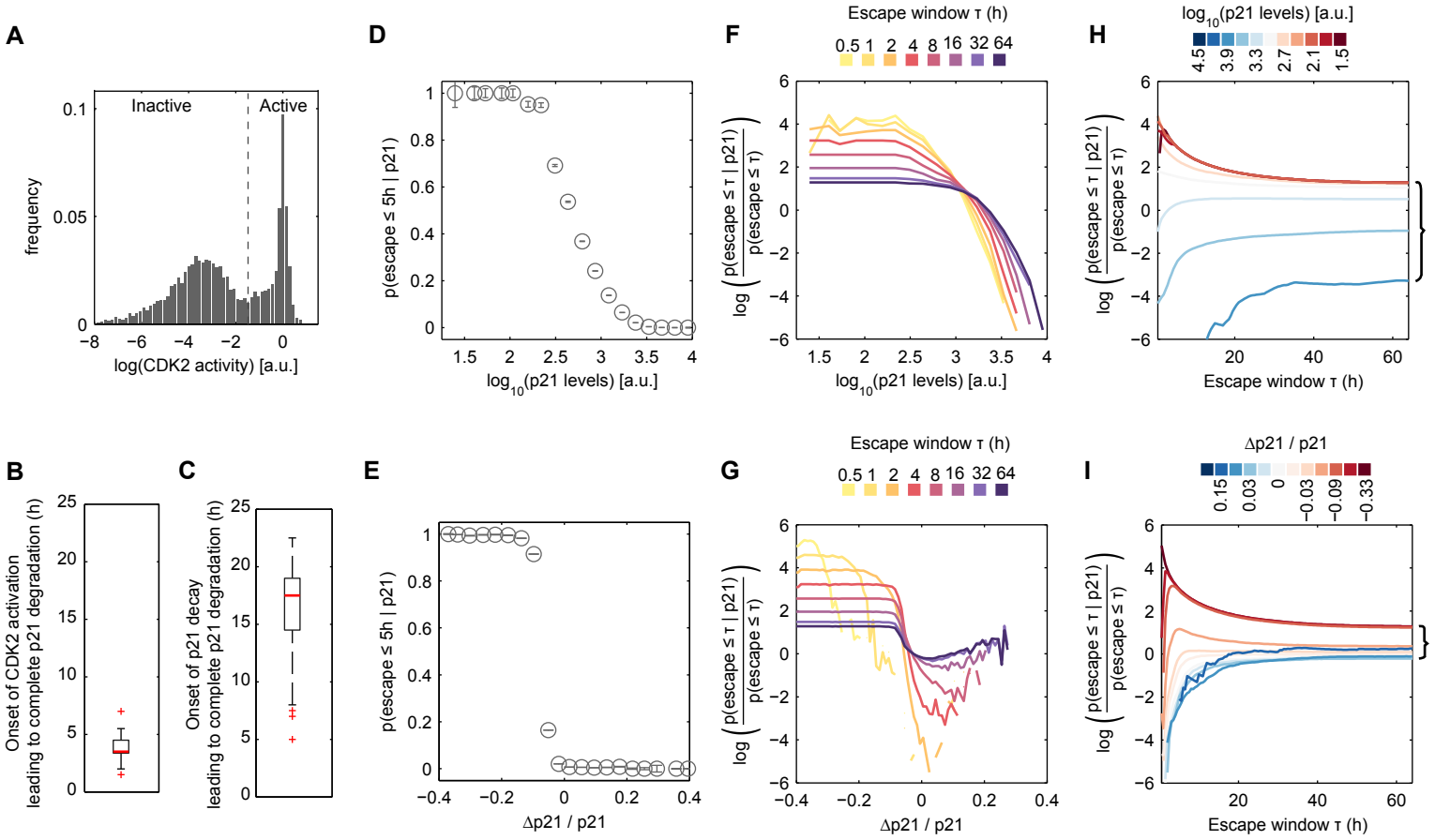

Figure S5. Estimation of escape probability from single cell p21 trajectories. *(Related to Main Text Figure 4)*

(A) Distribution of CDK2 activity (DHB-mVenus cyt/nuc ratio) in the vicinity of escape events. Dotted line defines a threshold to distinguish an active versus inactive state.

(B) Distribution of time from CDK2 activation to p21 degradation.

(C) Distribution of time of onset of persistent degradation of p21 before G1-S transition. Escapers start degrading p21 (negative derivative) before CDK2 activation. Once CDK2 becomes active, the rate of p21 degradation accelerates, as shown in Main Text Figure 4.

(D) Probability of escape within 5h as a function of p21 levels. Error bars represent standard error of probability estimates from 30 bootstrap pseudosamples of cells.

(E) Probability of escape within 5h as a function of p21 fold change (Δp21/p21). Error bars represent standard error of probability estimates from 30 bootstrap pseudosamples of cells.

(F) Probability of escape within τ hours as a function of p21 levels. Probabilities conditioned on p21 were normalized by the marginal probability of escape for each τ.

(G) Probability of escape within τ hours as a function of p21 fold change (Δp21/p21). Probabilities conditioned on p21 were normalized by the marginal probability of escape for each τ. Discontinuities in curves occur when the probability of escape for a given p21 fold change is 0.

(H) Probability of escape given p21 levels as a function of the escape window τ. Heterogeneity in p21 levels is most informative over short timescales and is stabilized over longer timescales.

(I) Probability of escape given p21 fold change (Δp21/p21) as a function of the escape window τ. Heterogeneity in p21 levels

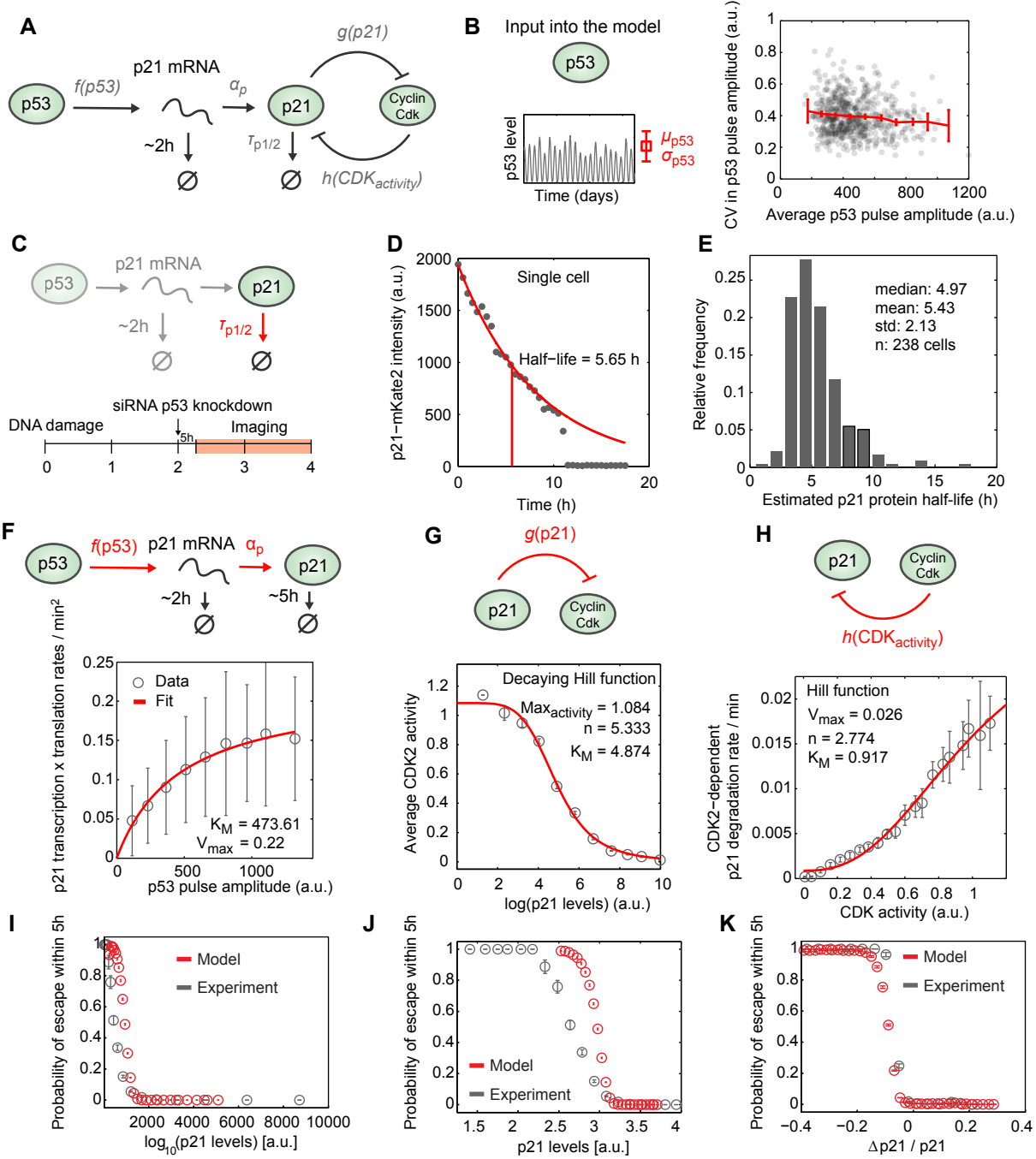

Figure S6. Experimental estimation of parameters for quantitative model. *(Related to Main Text Figure 5)*

(A) Schematic of quantitative model.

(B) Model receives a stochastic series of p53 pulses of fixed period and variable amplitude as an input. Average and CV p53 pulse amplitude were estimated from individual cell trajectories.

(C) Experimental timeline used to quantify p21 protein half-life in live individual cells. Cells received DNA damage and p53 was depleted using siRNA 2 days post-irradiation. Imaging started 5h post-knockdown. Images were taken every 30min.

(D) Representative trajectory of p21-mKate2 decay. Half-life was estimated by an exponential fit that excluded the of sharp p21 degradation corresponding to the G1-S transition.

(E) Distribution of p21-mKate2 half-life as quantified in (D).

(F) p53-dependent p21 production. The mean product of p21 transcription and translation rate as a function of p53 is shown. Error bars represent standard deviation. Red line is the best fit to a Michaelis-Menten functional form.

(G) p21-dependent average CDK2 activity. Error bars represent standard error of the mean. Red line is the fit to a decaying function.

(H) Estimate of CDK2-dependent p21 degradation rate. Error bars represent standard error of the mean. Red line is the fit to a function.

(I-K) Probability of escape within 5h as a function of p21 levels (I-J) or relative change in p21. Curves directly compare results from experimental data as shown in Figure S5 and results from simulations.

SUPPLEMENTAL TABLES

Table S1. Parameters implemented to model the interaction between fluctuations in p53 signaling and p21/CDK2 double negative feedback *(Related to main text Fig. 5).* Simulations are carried out in arbitrary concentration units (U).

Parameter	Definition	Value	Units
α_1	Maximum p21 transcription rate	0.22	min^{-1}
K_0	K_M of p53 dependent p21 transcription	473.61	U
α_2	p21 protein production rate	1	min^{-1}
α_3	Maximum CDK2 activity	1.084	
β_1	p21 mRNA degradation rate	0.0058	min^{-1}
β_2	Basal p21 protein degradation rate	0.0023	min^{-1}
β_3	Maximum rate of CDK2 induced p21 protein degradation rate	0.026	min^{-1}
K_1	K_M of p21-dependent CDK2 inhibition	4.784	U
K_2	K_M of CDK2-dependent p21 degradation rate	0.917	
n_1	Hill coefficient describing ultrasensitivity of p21-dependent CDK2 inhibition	5.333	
n_2	Hill coefficient describing ultrasensitivity of CDK2-dependent p21 degradation rate	2.774	
m	Average of p53 pulse amplitude distribution	250-700	U
CV	CV of p53 pulse amplitude	0.4	U
T	Period of p53 pulses	5	h
λ	Scaling of CDK2 dependent p21 degradation	30	